Workshop on Visualisation in Environmental Sciences (EnvirVis) (2021)
S. Dutta and K. Feige and K. Rink and D. Zeckzer (Editors)

Uncertainty-aware Detection and Visualization of Ocean Eddies in Ensemble Flow Fields - A Case Study of the Red Sea

F. Raith[1], G. Scheuermann[1] and C. Gillmann[1]

[1]Institute of Computer Science, Leipzig University, Germany

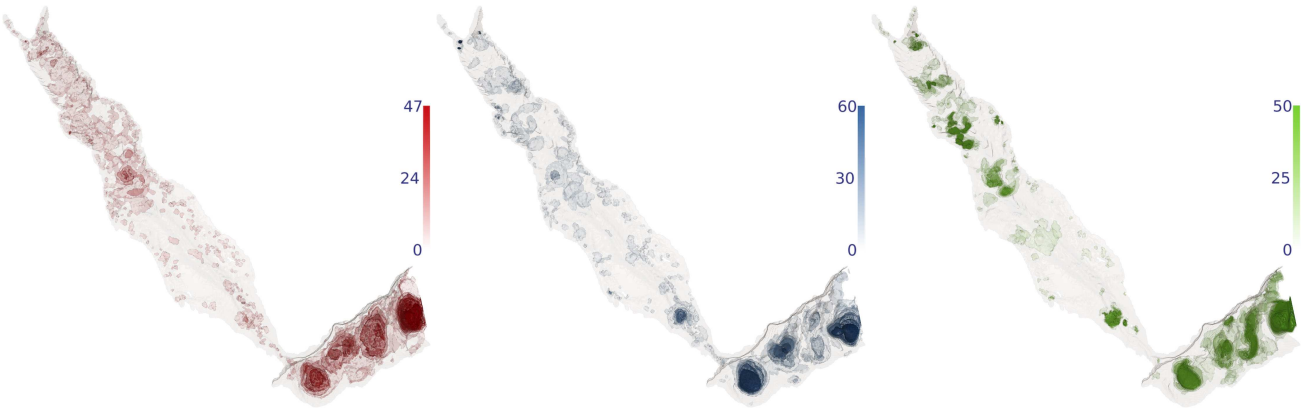

(a) (b) (c)

Figure 1: *Types of uncertainty in ocean eddy detection quantified and utilized for visualization in the presented work. Transparency encodes the amount of uncertainty detected in each cell of the ocean simulation where high transparency represents high uncertainty. a) Ensemble uncertainty. b) Time uncertainty. c) Parameter uncertainty. The colors will be used throughout the manuscript to provide consistency.*

Abstract

Eddy detection is a state of the art tool to examine transport behavior in oceans, as they form circular movements that are highly involved in transferring mass in an ocean. To achieve this, ocean simulations are run multiple times, and an eddy detection is performed in the final simulation results. Unfortunately, this process is affected by a variety of uncertainties. In this manuscript, we aim to identify the types of uncertainty inherent in ocean simulations. For each of the identified uncertainties, we provide a quantification approach. Based on the quantified uncertainties, we provide a visualization approach that consists of domain embedded views and an uncertainty space view connected via interaction. We showed the effectiveness of our approach by performed a case study of the Red Sea.

Keywords: *Eddy Detection, Uncertainty-aware Visualization*

1. Introduction

Ocean eddies are clockwise or counter-clockwise circular movements of water. They play an essential role in transferring heat, energy, and material in oceans and can affect global ocean dynamics, weather conditions, and commercial activities [Mcw08]. The detection of eddies is an important task to investigate oceanic dynamics, improve local ocean forecasts, and provide tools for the coastguard to undertake search-and-rescues [LYD*20].

To detect eddies, simulations of ocean water are run, and there exist a variety of techniques that aim to compute if an eddy is present in a particular cell of the simulation. This process introduces various uncertainties that can influence the decision-making process [SSK*16].

DOI: 10.2312/envirvis.20211080

To create an awareness of all these uncertainties, suitable visualization approaches are required. Unfortunately, they often do not include uncertainty or solely consider one type of uncertainty (see Section 2).

This work aims to provide an uncertainty-aware detection and visualization framework that allows incorporating uncertainties in eddies' simulation process. First, we provide a list of uncertainties in ocean simulation data (see Section 3). Based on this analysis, we provide mathematical mechanisms to quantify these uncertainties. At last, we provide a visualization approach that shows the computed eddies and the uncertainty in this process (see Section 4). The visualization consists of two views: a domain-embedded view showing the spatial location of detected eddies and the quantified uncertainties, and an uncertainty space view indicating the distribution of uncertainty quantified in a dataset. The views are connected via interaction.

Therefore, this paper contributes:

- An analysis of sources of uncertainties in ocean eddy detection
- A quantification approach for different sources of uncertainty in ocean simulations
- An uncertainty-aware visualization approach for ocean eddies

To show the benefits of the presented approach, we use the SciVis 2020 Contest holding an ocean simulation of the Red Sea, which consists of multiple time-dependent samples, and apply our uncertainty-aware detection and visualization of eddies to it (see Section 5). Our results will be discussed in Section 6.

2. Related Work

In this section, we aim to provide an overview of eddy detection approaches and uncertainty analysis in this context. Ocean eddies play an important role. They provide essential material knowledge for the equilibrium balances of the general circulation and climate. There is a direct link between the water mass properties of an eddy and its rotation. Warm eddies rotate anti-cyclonically, while cold eddies rotate cyclonically [SYY*13].

2.1. Eddy Detection and Visualization in General

Ocean eddies can be detected in various manners [LSW*19]. Here, Wavelet methods [DBSL07] or Vector-based methods [NDD*10] are common approaches. The most popular Eddy detection approach is based on the Okubo–Weiss parameter (W) [Oku70, Wei91]. For example, in the work of Raith et al. [RRHS17] W is used to detect eddies and track their transport properties of temperature and salinity over time.

The detection and visualization of eddies are highly related to ensemble visualization, where Wang et al. [WHLS18] provided a state of the art analysis. On the other hand, eddy detection and visualization is a clear application of flow field visualization as shown in the state of the art report by Bujack and Middel [BM20] which can be either performed by partitioning-based techniques [SLWS08] or structure-based techniques [SJdTWS07].

Xie et al. [XLWD19] provided a state of the art analysis of ocean data visualization, where uncertainty analysis and its visualization have been stated as one major challenge when dealing with ocean data. This forms the motivation of the presented work.

There exists a variety of visualization approaches that can be used to indicate eddies. They include iso-surface based approaches [WZW*20], glyph-based approaches [FEFH20], visual analytics dashboards [HCA*20], feature tracking approaches [OBH*20] and web-based visualizations [VPD20].

Unfortunately, these approaches are not aware of the different sources of uncertainty inherent in an ocean simulation and are not able to compute or present them. In the presented approach, we aim to identify sources of uncertainty in ocean simulation data and provide methods to compute them.

2.2. Uncertainty-aware Eddy Detection and Visualization

The detection of eddies in ocean simulation is highly affected by uncertainty, which has been visually tackled, as summarized below.

Gillmann et al. [GWHH18] provided a surface extraction algorithm that can be used to show the difference in the boundary of detected eddies, which can also be visualized [GWHA18]. Franz et al. [FRM*18] used a Bayesian neural network to detect eddies and a probability for each eddy. Here, eddies are shown with different transparencies according to the predicted probability. Unfortunately, this approach does not include multiple simulation runs into their considerations.

Athawale et al. [AAEJ20] used statistical rendering to indicate how often an eddy can be detected in a simulation. Their visualization shows a lower alpha-value when eddies are detected less often in the available simulations. Höllt et al. [HMZ*14] provided a visual tool that allows to examine the detection of ocean eddies in ensemble visualizations and review the size of individual eddies. Although these approaches provide visual feedback for the occurrence of eddies in an ensembles, they do not address further uncertainties such as parameter uncertainty or transport uncertainty.

Zanna et al. [ZBH*18] provided a side-by-side visualization that shows the transport uncertainty that can be computed based on a prior eddy detection. Here, color coding is indicated to show uncertain areas in predicted transport. Rapp and Dachsbacher [RD20] generalized this approach for various transport examinations that are not restricted to eddies. Unfortunately, these approaches do not consider the uncertainty of the eddy computation itself.

Although the presented approaches can indicate one source of uncertainty in a visualization, they cannot indicate multiple sources. This forms the basic research motivation of our approach.

3. Uncertainties in Eddy Detection

The process of detecting eddies is affected by a variety of sources of uncertainty. This uncertainty highly affects the decision-making process based on ocean water simulations. In this section, we aim to summarize these uncertainties and discuss them.

The *uncertainty* of a measurement is a quantification of the doubt about the measurement result [HDF10]. If this uncertainty is known, the measurand is defined as *uncertainty-aware*. In contrast, if this uncertainty is unknown, a measurand is *uncertain*.

This doubt can originate from a variety of effects, including an incomplete definition of the measurand, the imperfect realization of the definition of the measurand, non-representative sampling, inadequate knowledge of the effects of environmental conditions on the measurement or imperfect measurement of environmental conditions, personal bias in reading analog instruments, finite instrument resolution or discrimination threshold, inexact values of measurement standards, reference materials and parameters, approximations and assumptions incorporated in the measurement method and procedure, and variations in repeated observations of the measurand under apparently identical conditions [BHP15].

These effects can be separated into different *categories*: uncertainty based on the underlying model (epistemic uncertainty *e*) or statistical uncertainty resulting from variations in the measurement result when running an experiment multiple times (aleatoric uncertainty *a*). Here, a model refers to a computational description that tries to map physical dependencies as adequately as possible. Naturally, a model is never complete, as the knowledge about the physics surrounding us is not complete as well. In most cases, aleatoric uncertainty is usually the type of uncertainty requested to be visualized to enhance a decision-making process in a given application [PRJ12].

3.1. Sources of Uncertainty in Eddy Detection

In the context of ocean simulation, multiple sources of uncertainties can affect the resulting data and their analysis, which will be summarized in the following where each type of uncertainty is classified as epistemic or aleatoric.

Ensemble Uncertainty (*a*) Ocean simulations are run multiple times using different boundary conditions including temperature, amount of water, or flow conditions. This results in a set of potential ocean behaviors captured. Unfortunately, it is not clear if a simulation is more trustworthy than another. Here, all simulations need to be considered, resulting in ensemble uncertainty. For eddy computations, this means that there might be simulations that contain an eddy at a certain point and others that do not.

Time Uncertainty (*a*) Ocean simulation results usually yield a time-series that needs to be analyzed. Throughout different time steps, the values can be more or less accurate, and time steps need to be correlated to understand eddies detected in different time steps. This results in time steps that can be classified as certain or uncertain, defined as time uncertainty.

Parameter Uncertainty (*e*) When detecting eddies, ocean simulations are examined mathematically to determine if an eddy is present at a specific location or not. Here, several parameters can be used to set a threshold that aims to exclude noise resulting in false detection of eddies. These thresholds are chosen based on several experiments, and there exists a broad consensus about proper thresholds. Still, there is no mathematical proof of an optimal threshold. This results in parameter uncertainty.

3.2. Requirements for Visualization of Uncertainty-aware Eddies

Sacha et al. [SSK*16] provided guidelines that need to be considered in order to create an uncertainty-aware visualization in general. We would like to derive criteria for uncertainty-aware visualization approaches for eddy computation in ocean simulations for this work.

R1: Quantify Uncertainty in each Instance In eddy detection tasks, ocean simulation results need to be quantified according to their uncertainty. This mainly refers to the aleatoric types of uncertainty and includes ensemble uncertainty as well as the time uncertainty in the case of eddy detection.

R2: Propagate Uncertainty throughout a Computation For eddies, a variety of metadata can be defined, such as size, location of the center, or transport properties. The computation is based on the uncertainty-aware input resulting from **R1**, which leads to uncertain properties. Here, proper accumulation and propagation approaches need to be considered.

R3: Visualize Uncertainty in each Instance Based on the quantification and propagation of uncertainty in **R1** and **R2**, ocean simulations can be extended. Here, the ocean simulation obtains an additional value for each quantified type of uncertainty. These quantities need to be visualized to allow users to access them. This can easily result in clutter if visual variables are not chosen properly.

R4: Provide suitable Interaction Based on **R3**, users need to be enabled to interact with the created uncertainty-aware visualization approach. Here, suitable interaction metaphors need to be selected to provide easy access to the data itself and the uncertainty quantification.

4. Uncertainty-aware computation and visualization of eddies

This section provides uncertainty quantification approaches for the identified sources of uncertainty in Section 3. Based on these computations, we provide an uncertainty-aware Eddy visualization. The only input required for the eddy calculation is a velocity field defined on the corresponding domain.

4.1. Eddy Detection

The most popular Eddy detection approach is based on the Okubo–Weiss parameter (W) [Oku70, Wei91]. This criterion quantifies the relative importance of deformation and rotation. This can be computed by:

$$W = \underbrace{s_n^2 + s_s^2}_{strain-dominated} - \underbrace{\omega^2}_{vorticity-dominated}, \tag{1}$$

where s_n is the normal strain that indicates currents that are running against each other. s_s defines the shear strains that determine currents that are running in opposite directions. ω is defined as the vorticity, where currents are moving in different directions. More precise these components can be computed as:

$$s_n = \frac{\delta u}{\delta x} - \frac{\delta v}{\delta y}, \quad s_s = \frac{\delta v}{\delta x} + \frac{\delta u}{\delta y}, \quad \omega = \frac{\delta v}{\delta x} - \frac{\delta u}{\delta y} \tag{2}$$

Here, u defines the east-west velocity component, v describes the

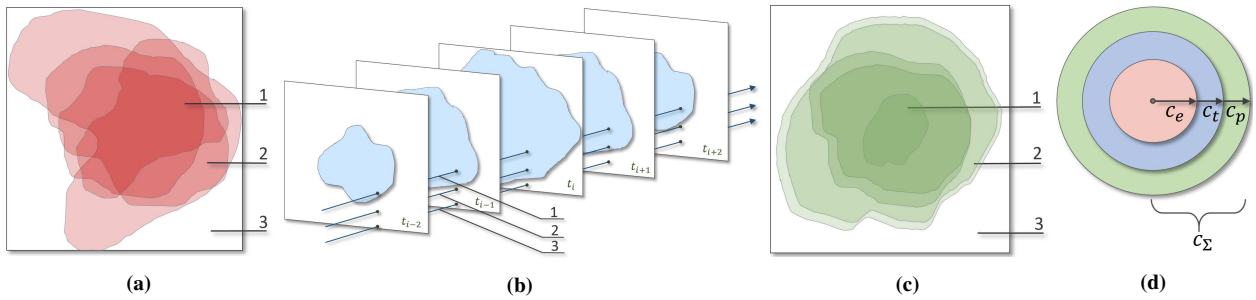

Figure 2: *Quantification of sources of uncertainty contained in ocean simulation data and the creation of the glyph that represents the quantities. Depending on the examined axis, it can be certain (1) that an eddy is present, uncertain if an eddy is present (2) and certain that an eddy is not present (3) a) Ensemble uncertainty u_e. b) Time uncertainty u_t. c) Parameter uncertainty u_p. d) The quantification of the three uncertainties combined in a disk glyph. The resulting size of the glyph depends on u_Σ.*

north-south components and x and y describe locally east-pointing and west-pointing vectors. Defining eddies in this way allows them to entirely local. Resulting from this, it is a proper choice for big data such as ocean simulations.

As shown in Equation 1, W can be separated into two parts: positive strain-dominated domains and negative vorticity-dominated domains. Still, the numbers close to zero are mostly dominated by noise. Here, a threshold is applied that only keeps points with negative Okubo-Weiss values and discarding the values that are close to zero. Therefore, the threshold should be nonzero. In the ocean analysis community, Okubo-Weiss values are divided by their standard deviation σ. This results in keeping meaningful data points that are located at least 0.2 standard deviations from 0. We keep this scheme to provide a suitable starting point for our analysis while considering this assumption to be affected by uncertainty. More formally, this means:

$$\frac{W}{\sigma_W} \leq -0.2 \tag{3}$$

Still, W detects too many false positive eddies, which raises the need of a further evaluation [RRHS17]. This can be achieved by the so-called *four-corner method*. This method checks if an eddy is rotating completely. This is achieved by computing an angle between each velocity vector of the points in the eddies and a vector oriented towards the east. The angles are sorted into four classes: 0 - 89°, 90 - 179°, 180 - 269°, 270 - 360°. Each angle range needs to be present in an eddy to a certain percentage. We use 8% as defined by Williams et al. [WHP*11].

Also, we compute the center c of the eddy, which we use to position visual variables in Section 4.3. In this work, the center c corresponds to the local minimum in the Okubo-Weiss field of the respective eddy. Our considerations regarding the quantification of uncertainty will build upon this eddy detection approach.

4.2. Computation of Uncertainty

In Section 3, we determined the uncertainties that affect the computation and visualization of eddies. In the following, we provide quantification approaches for each of these uncertainties. In this setting, we aim to compute different settings of eddy detection, while varying different input parameters. While testing, we aim to capture how often we found an eddy using these different parameters. As a measure of uncertainty, we aim to express the occurrences of an eddies in comparison to the number of processed tests. For the considered sources of uncertainty, we can make the following definitions:

- r_i, range of parameters, where eddies are detected
- $min(r_j)$, $max(r_j)$, $step(r_j)$ the minimum, maximum, and step size in r_i
- p_i, number of present eddies in r_i
- $max(p_i)$, the maximum from p_i of all cells from one eddy in a simulation run
- $i \in \{e,t,p\}$

where e refers to ensemble uncertainty, t refers to time uncertainty, and p refers to parameter uncertainty.

An overview can be found in Figure 2. Here, the resulting uncertainty can be formulated as follows:

$$u_i = 1 - \frac{max(p_i) * step(r_i)}{max(r_i) - min(r_i)} \tag{4}$$

And equivalently we computed certainty as follows:

$$c_i = 1 - u_i \tag{5}$$

Ensemble Uncertainty u_e aims to provide a measure that captures the uncertainty of eddy detection when considering multiple simulation runs. Figure 2a shows a schematic description of eddies evolving in ensembles. Here, we count the number of simulations where an eddy can be detected. Therefore, $r_e = [0,n]$, where n is the number of simulations that is considered. Naturally, $step(r_e)$ is set to 1 to include the entire ensemble dataset. Figure 1a shows p_e, where the opacity of the red color indicates the amount of found eddies throughout the different ensembles. Here, we can clearly identify four major eddies in the right part, whereas the left part seems to be uncertain in terms of eddy detection.

Time Uncertainty u_t To capture time uncertainty, we need to

review different time steps and compare the found eddies. Here, $r_t = [0, t_{max}]$, where t_{max} holds the maximum number of time steps. To include all time steps, $step(r_t)$ is set to 1. Figure 2b shows a scheme how eddies evolve throughout time. Based on this, Figure 1b shows p_t, where only three major eddies can be found in the right part of the sea. On the other hand, we can identify an eddy on the left side of the Red Sea, which is very certain considering time.

Parameter Uncertainty u_p To capture the parameter uncertainty of an eddy detection, we need to alter the used threshold that discards eddies resulting from noisy data. Although this is not the only parameter that can be changed, we would like to focus on the threshold that excludes noisy data. Other thresholds can be considered in this analysis in the same manner but need to be tested for independence. Figure 2c shows a scheme how eddies evolve using different input parameters. As already mentioned, $\frac{W}{\sigma_W} \leq -0.2$ is a common use of a threshold for eddies. Here, we can alter the threshold. Although the range can be set arbitrarily, solely values between $-\inf$ and 0.0 are suitable for the given use case. The selected step size defines how extensive the analysis of the parameter uncertainty is performed. Figure 1c shows p_p encoded in the transparency of green. In this case, separating the four major eddies in the right part of the sea is not clear. Still, it is very certain that the simulation ensemble contains multiple smaller eddies in the left part.

Combination of Uncertainties u_Σ As shown in Figure 1, each type of uncertainty can be reviewed independently by mapping p into the original domain. Still, this could result in visual clutter. In addition, we aim for a unified measure that captures all three types of uncertainty. Therefore, the unified uncertainty u_Σ can be computed as follows:

$$u_\Sigma = \frac{\Sigma_i u_i}{3} \tag{6}$$

And equivalently we computed unified certainty as follows:

$$c_\Sigma = \frac{\Sigma_i c_i}{3} \tag{7}$$

This means, that we aim to add all measured uncertainties and rescale them back into the range of $[0, 1]$, where 1 means, that the eddy is completely uncertain and 0 means, that the eddy is absolutely certain and vice versa for the unified certainty.

In this manuscript, we did not consider if the examined uncertainties are independent. We aimed to provide a first attempt to understand different types of uncertainty in eddy detection. In fact, the made computation is a worst case estimation of the three combined uncertainties. Also further combination errors such as the $L2$-Norm can be applied when assuming, that the considered uncertainties are independent. The shown computations will be used in the following to provide an uncertainty-aware visualization of eddies.

4.3. Visualization

Based on the performed uncertainty quantification, we are able to provide an uncertainty-aware visualization of eddies. We provide two views: a *domain-embedded view* and an *uncertainty space view*, that are connected via *interaction*.

4.3.1. Domain-embedded View

The domain-embedded view shows the underlying domain that is considered in the detected ocean eddies. This domain is used to provide a spatial location of the detected eddies and their quantified uncertainties. Our goal is to extend the display of detected eddies by a glyph that captures the three types of uncertainty that have been quantified. These glyphs allow us to see at a glance how likely the eddy is and how strong different types of uncertainty are in relation to others. Thereby, the probability corresponding to all uncertainty sources considered in this paper is displayed. First, we provide an iso-surface-based visualization of eddies, where the opacity of each iso-surface is based on u_Σ. In this iso-surface, we place a glyph consisting of three disks that are placed into each other. All disks hold the same height, which can be adjusted according to the users need. The position is determined by c. The extent of each area in the glyph sees Figure 2d indicates the magnitude of each certainty c_i. Here, each disk varies its size according to the ratio that the respective uncertainty holds in the combination of uncertainties. The total size of the glyph shows the combined magnitude.

It is also possible to display the glyph size normalized, which simplifies comparing the respective sources of uncertainty with each other. The user can choose whether the uncertainty of a single uncertainty source or the united uncertainty u_Σ is used in Figure 3.

Figure 3: *Domain-embedded view of the presented approach. Eddies are shown by iso-surfaces that encode uncertainty in their transparency. Each eddy obtains a glyph that indicates the distribution of the three quantified uncertainty in each eddy.*

4.3.2. Uncertainty Space View

In contrast to the domain-embedded view, the uncertainty space view spans an attribute space consisting of the three uncertainty sources described in this paper. In this space, the entire domain or only a part of it is mapped linearly. Here, we build an uncertainty-cube that consists of the three uncertainty values as dimensions. In the respective cube, all uncertainties will be shown as points in space, where each uncertainty describes one coordinate (x, y, z), to provide a first overview of the distribution of uncertainty values in a dataset. This visualization is helpful in understanding which uncertainty combinations can be examined.

4.3.3. Interaction

The interaction serves to connect the two views and offer a further possibility of analysis. The approach to interaction is based on the

work [RBN*18, BRS*19, RBR*20] on fiber-surface extraction in which regions from a co-domain are mapped into a domain and vice versa with an region of interest (ROI). For this purpose, users can identify regions that should be examined more closely with different types of ROI. In this cases, the extraction of the fiber-surface takes less than 1s. The domain, defining the ROI, or partial domain, is represented as a wireframe, as shown in Figure 5a. Applied to our work, we can enable the user to examine the entire uncertainty space and display the results in addition to the detected eddies in the domain-embedded view see Figure 5b.

On the other hand, the user can select a single eddy in the domain-embedded view and display it in the uncertainty space see Figure 5c. The user can then examine the eddies' details in the uncertainty space view and project them back into the domain-embedded view see Figure 5d. In this study, the use time was not considered. Still, we expect a certain amount of training time to handle this interaction usefully.

5. Case Study

To show the effectiveness of the presented approach and discuss it, we provided a case study of the Red Sea, which is a freely available dataset that was published by the SciVis Contest 2020.

5.1. Data

The examined dataset shows a bathymetry of the Red Sea over a variety of time steps and ensembles. In addition, the dataset holds different types of uncertainty that will be summarized by the presented approach.

The dataset consists of the Red Sea bathymetry and an ensemble (50 members) of time-dependent 3D flow and scalar fields on a regular grid. Each simulation consists of 60 time steps, where each time step contains an ensemble of 50 samples defined on a regular grid with the size of 500x500x50 cells. Each cell has a size of 0.04° x 0.04° (4km) with 4m height at the surface, increasing to 300m near the ground. Each cell in the simulation contains the following information: satellite sea surface temperature, sea level anomalies and in situ salinity, and temperature [STZ*20].

5.2. Results

To apply our approach to the presented dataset, we first need to define the used ranges for the uncertainty computation. Here, we set $r_e = [0,50]$ with $step(r_e) = 1$, $r_p = [-0.01,-0.5]$ with $step(r_p) = 0.01$ and $r_t = [0,60]$ with $step(r_t) = 1$. Then, we start a simulation run to detect the eddies in the Red Sea MEAN dataset at time step 0 with a percentage of 8% for the four-corner method and -0.2 as the threshold for W.

Figure 4 shows two closeups of the domain-embedded visualization. Figure 4a mainly shows the Gulf of Aden, where usually 4 major eddies are detected. Applying our visualization approach shows that the Eddy 2 and Eddy 3 hold a high uncertainty, as they are shown more transparent than the other eddies. This indicates that the eddies are less certain than Eddy 1 and Eddy 4. This is also indicated by the size of the glyph. Here, the glyphs of the uncertain

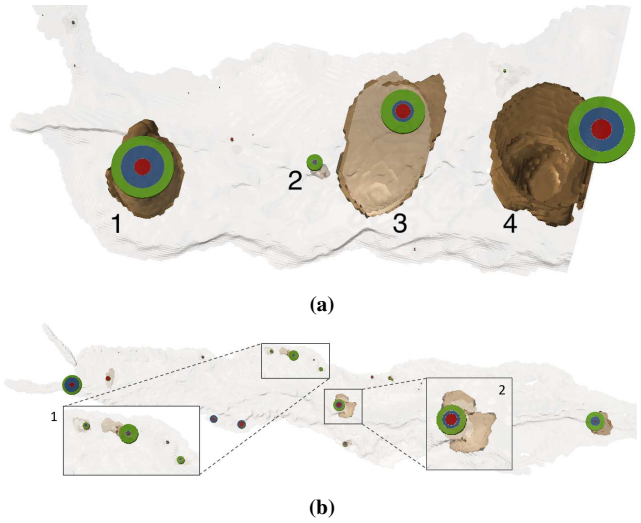

Figure 4: *Two closeups of the domain visualization shown in Figure 3. a) Closeup of the Gulf of Aden. b) Closeup of the Red Sea with two sub closeups (marked as 1 and 2).*

eddies are smaller. When having a closer look at the glyphs, we can determine that the three uncertainties are well distributed among the three captured uncertainties in certain glyphs. When considering Eddy 2, we can directly see that the u_p is very high in comparison to the remaining uncertainties. This indicates that the parameter choice of W is very sensitive in this eddy detection. For Eddy 3, we can see that the overall high uncertainty mainly origins from the parameter uncertainty and the ensemble uncertainty, whereas time does not introduce a high amount of uncertainty. Figure 4b shows a closeup of the Red Sea. We can easily identify that all detected eddies hold a high uncertainty, as they are shown very transparently, and the resulting glyphs are relatively small. Closeup 1 shows a set of small eddies that hold a high uncertainty. For all these eddies it can be seen that the parameter uncertainty is very high in comparison to the remaining uncertainties. This indicates a high sensitivity of W in these selected eddies. Closeup 2 shows an eddy with an intermediate amount of uncertainty. Here, we can directly see that this uncertainty origin from a mix of high u_e and high u_p, whereas time does not seem to have a strong influence on the uncertainty of the eddy. This shows that the proposed visualization allows an easy mechanism to understand the uncertainty inherent in an eddy and the distribution of uncertainty throughout the different uncertainties. Here, users can easily separate eddies into different groups.

Figure 5a shows the selection process in the co-domain. Here, a plane is used as a selection tool. Reviewing the first eddy of the Gulf of Aden in the domain-embedded space, we can identify a core of the eddy as shown in orange in Figure 5b. This core indicates the most temperature color-coded in orange. This is an important information for domain scientists as properties such as temperature and salt content can provide a deeper understanding of ocean dynamics.

Figure 5c shows the selection in the co-domain using two cubes (marked as 1 and 2). Please note that the domain is pre-selected by using the fourth eddy in the Gulf of Aden. The respective areas of

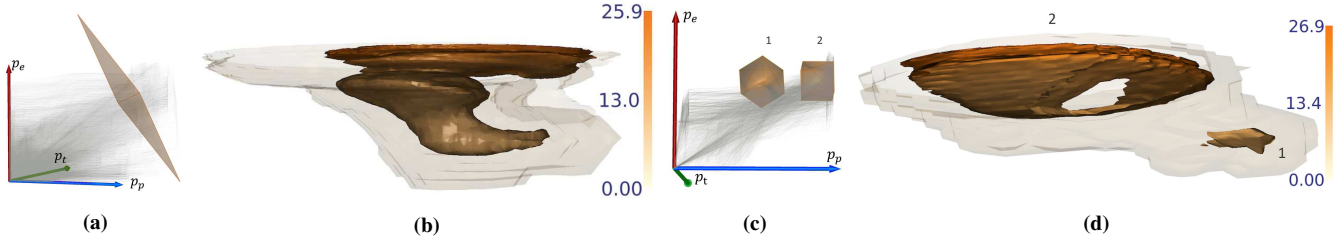

Figure 5: *Visual exploration of uncertainty space of ocean eddy computation. a) Selection of uncertainty space via the co-domain using a selection plane. b) Resulting selection in the domain space for the fourth eddy in the Gulf of Aden. c) Pre-selection of co-domain using the Eddy 1 in the Gulf of Aden and two additional selection cubes. d) The two selected cubes highlighted in the domain-embedded view of the Gulf of Aden. The selected parts of the eddies are color-coded according to the temperature present in the simulation result.*

selection can be reviewed in Figure 5d. Here, we can see a separation of these two areas that result in two compartments in the eddy. Cube 1 shows a smaller subdomain holding a high ensemble uncertainty. In addition, the selected core itself holds a high uncertainty. Cube 2 shows high uncertainty in all three quantified uncertainties and is located in the center of the eddy. This shows that the larger core of the eddy is more certain than the smaller eddy attached to it. Again, the temperature at the considered cell in the simulation is used as a color-coding.

This example shows that the interaction approach we propose allows users to explore the distribution of uncertainties throughout the selected eddies and correlate them with the defined uncertainty space.

6. Discussion

In this manuscript, we provide an visualization approach to capture different sources of uncertainty inherent in the computation of ocean eddies and conducted a case study of the Red Sea. In this section, we aim to discuss the presented approach.

6.1. Check of Requirements

In section 3, we provided a list of requirements that need to be fulfilled in order to provide an uncertainty-aware visualization of eddies.

We quantified three different types of uncertainty (containing both aleatoric and epistemic uncertainty) that are inherent in detected eddies. Here, we provide suitable quantification approaches for ensemble uncertainty, time uncertainty, and parameter uncertainty (R1). We are aware that more sources of uncertainty might be considered in this context, such as user bias or sampling uncertainty. Still, we decided to focus on uncertainties that are directly originating from the computational results of the eddy detection. In the presented case, we restrict the uncertainty analysis to an uncertainty-aware detection and visualization of eddies. Further analysis of eddies is explicitly not covered in this work due to scope restrictions. Therefore, R2 can be neglected in the presented analysis.

We provided an uncertainty-aware visualization that allows visualizing eddies and their uncertainties based on the preformed uncertainty quantification. Here, we combined all quantified uncertainties into one visualization that shows the total amount of uncertainty as well as the distribution of uncertainty among the different kinds. As we can include this knowledge into a general visualization of eddies, we allow users to review detected eddies and their uncertainty (R3). In addition, we provide an uncertainty space cube that shows the distribution of detected uncertainties.

Between the two visualization approaches, we provide an interaction by brushing and linking (R4). Here, users can visually inspect the uncertainty space that results from our analysis and defines subspaces that they need to visually correlate with the 3D view. The same can be achieved when selecting an eddy. Here, respective areas in the uncertainty space will be highlighted.

6.2. Further Applications

Although we provided very specific ocean eddies analysis, our approach is not restricted to ocean data in general. Whenever turbulences are of interest, our visualization approach can help to examine these structures. We also propose that an analysis of uncertainties in geospatial data is a need in many applications, especially when considering multiple ensembles. Here, our approach could be seen as an example of performing uncertainty analysis in the respective areas.

7. Conclusions and Future Work

We proposed an uncertainty-aware detection and visualization approach of ocean eddies in ensemble flow fields. Our approach is based on a brief introduction to types of uncertainty that are present in ocean simulations. Followed by that, we utilize the Okubo-Weiss eddy detection approach to extract eddies. For each source of uncertainty, we provided a quantification of each type of uncertainty. At last, we provide a visualization approach that provides a holistic view of the quantified uncertainties. We conducted a case study of the Red Sea and examined the eddies and their uncertainty based on the quantified uncertainties.

For future work, we aim to provide further uncertainty quantification approaches for meta-parameters that can be computed for certain eddies. In addition, we aim to analyze further datasets that contain ocean simulations. At last, we target a user evaluation that examined the performance of the interaction methodology provided

References

[AAEJ20] ATHAWALE T. M., A. ENTEZARI B. W., JOHNSON C. R.: Statistical rendering for visualization of red sea eddy simulation data. IEEE Scientific Visualization Contest 2020. 2

[BHP15] BOUMANS M., HON G., PETERSEN A. C.: *Error and uncertainty in scientific practice*. Routledge, 2015. 3

[BM20] BUJACK R., MIDDEL A.: State of the art in flow visualization in the environmental sciences. *Environmental Earth Sciences 79*, 2 (2020), 1–10. 2

[BRS*19] BLECHA C., RAITH F., SCHEUERMANN G., NAGEL T., KOLDITZ O., MASSMANN J.: Analysis of coupled thermo-hydro-mechanical simulations of a generic nuclear waste repository in clay rock using fiber surfaces. In *2019 IEEE Pacific Visualization Symposium (PacificVis)* (2019), IEEE, pp. 189–201. 6

[DBSL07] DOGLIOLI A. M., BLANKE B., SPEICH S., LAPEYRE G.: Tracking coherent structures in a regional ocean model with wavelet analysis: Application to cape basin eddies. 2

[FEFH20] FRIEDERICI A., ENGELKE W., FALK M., HOTZ I.: Tracing eddy transport in the red sea and gulf of aden. IEEE Scientific Visualization Contest 2020. 2

[FRM*18] FRANZ K., ROSCHER R., MILIOTO A., WENZEL S., KUSCHE J.: Ocean eddy identification and tracking using neural networks. 2

[GWHA18] GILLMANN C., WISCHGOLL T., HAMANN B., AHRENS J.: Modeling and visualization of uncertainty-aware geometry using multivariate normal distributions. In *2018 IEEE Pacific Visualization Symposium (PacificVis)* (2018), pp. 106–110. 2

[GWHH18] GILLMANN C., WISCHGOLL T., HAMANN B., HAGEN H.: Accurate and reliable extraction of surfaces from image data using a multi-dimensional uncertainty model. *Graphical Models 99* (2018), 13–21. 2

[HCA*20] HAN X., CHENG S., AN Y., LU X., LI G., SHAN G., LIU H., LIN P.: Eddy-based visual analysis system for transport in the red sea. IEEE Scientific Visualization Contest 2020. 2

[HDF10] HASINOFF S. W., DURAND F., FREEMAN W. T.: Noise-optimal capture for high dynamic range photography. In *2010 IEEE Computer Society Conference on Computer Vision and Pattern Recognition* (June 2010), pp. 553–560. 2

[HMZ*14] HÖLLT T., MAGDY A., ZHAN P., CHEN G., GOPALAKRISHNAN G., HOTEIT I., HANSEN C. D., HADWIGER M.: Ovis: A framework for visual analysisof ocean forecast ensembles. *IEEE Transactions on Visualization and Computer Graphics 20*, 8 (2014), 1114–1126. 2

[LSW*19] LIAN Z., SUN B., WEI Z., WANG Y., WANG X.: Comparison of eight detection algorithms for the quantification and characterization of mesoscale eddies in the south china sea. *Journal of Atmospheric and Oceanic Technology 36*, 7 (01 Jul. 2019). 2

[LYD*20] LIANG S.-J., YOUNG C.-C., DAI C., WU N.-J., HSU T.-W.: Simulation of ocean circulation of dongsha water using non-hydrostatic shallow-water model. *Water 12*, 10 (2020). 1

[Mcw08] MCWILLIAMS J. C.: *The Nature and Consequences of Oceanic Eddies*. American Geophysical Union (AGU), 2008, pp. 5–15. 1

[NDD*10] NENCIOLI F., DONG C., DICKEY T., WASHBURN L., MCWILLIAMS J. C.: A vector geometry–based eddy detection algorithm and its application to a high-resolution numerical model product and high-frequency radar surface velocities in the southern california bight. *Journal of Atmospheric and Oceanic Technology 27*, 3 (2010), 564 – 579. 2

[OBH*20] OZER S., BEMIS K., HUA W., GOKTOGAN A., AYDOĞAN M., GUO K., KANG D., LIU L., SILVER D.: The use of 3D optical flow, feature-tracking and token-tracking petri nets to analyze and visualize multiple scales of ocean eddies. IEEE Scientific Visualization Contest 2020. 2

[Oku70] OKUBO A.: Horizontal dispersion of floatable particles in the vicinity of velocity singularities such as convergences. *Deep Sea Research and Oceanographic Abstracts 17*, 3 (1970), 445–454. 2, 3

[PRJ12] POTTER K., ROSEN P., JOHNSON C. R.: From quantification to visualization: A taxonomy of uncertainty visualization approaches. In *Uncertainty Quantification in Scientific Computing* (Berlin, Heidelberg, 2012), Springer Berlin Heidelberg, pp. 226–249. 3

[RBN*18] RAITH F., BLECHA C., NAGEL T., PARISIO F., KOLDITZ O., GÜNTHER F., STOMMEL M., SCHEUERMANN G.: Tensor field visualization using fiber surfaces of invariant space. *IEEE transactions on visualization and computer graphics 25*, 1 (2018), 1122–1131. 6

[RBR*20] RAITH F., BLECHA C., RINK K., WANG W., KOLDITZ O., SHAO H., SCHEUERMANN G.: Visual analysis of a full-scale-emplacement experiment in the underground rock laboratory mont terri using fiber surfaces. 6

[RD20] RAPP T., DACHSBACHER C.: Uncertain transport in unsteady flows, 2020. arXiv:2009.04531. 2

[RRHS17] RAITH F., RÖBER N., HAAK H., SCHEUERMANN G.: Visual eddy analysis of the agulhas current. In *Proceedings of the Workshop on Visualisation in Environmental Sciences* (2017), p. 25–29. 2, 4

[SJdTWS07] SALZBRUNN T., JÄNICKE H., DE THOMAS WISCHGOLL, SCHEUERMANN G.: The state of the art in flow visualization: Structure-based techniques. 2

[SLWS08] SALZBRUNN T., LEITTE H., WISCHGOLL T., SCHEUERMANN G.: The state of the art in flow visualization: Partition-based techniques. vol. 2008, pp. 75–92. 2

[SSK*16] SACHA D., SENARATNE H., KWON B. C., ELLIS G., KEIM D. A.: The Role of Uncertainty, Awareness, and Trust in Visual Analytics. *IEEE Transactions on Visualization and Computer Graphics 22*, 01 (Jan. 2016), 240–249. 1, 3

[STZ*20] SANIKOMMU S., TOYE H., ZHAN P., LANGODAN S., KROKOS G., KNIO O., HOTEIT I.: Impact of atmospheric and model physics perturbations on a high-resolution ensemble data assimilation system of the red sea, 2020. arXiv:2002.01825. 6

[SYY*13] SAITO R., YAMAGUCHI A., YASUDA I., UENO H., ISHIYAMA H., ONISHI H., IMAI I.: Influences of mesoscale anticyclonic eddies on the zooplankton community south of the western Aleutian Islands during the summer of 2010. *Journal of Plankton Research 36*, 1 (09 2013), 117–128. 2

[VPD20] VO H., PHAM V., DANG T.: Red sea eddies visualization for the web. IEEE Scientific Visualization Contest 2020. 2

[Wei91] WEISS J.: The dynamics of enstrophy transfer in two-dimensional hydrodynamics. *Physica D: Nonlinear Phenomena 48*, 2 (1991), 273–294. 2, 3

[WHLS18] WANG J., HAZARIKA S., LI C., SHEN H.-W.: Visualization and visual analysis of ensemble data: A survey. *IEEE Transactions on Visualization and Computer Graphics PP* (07 2018), 1–1. 2

[WHP*11] WILLIAMS S., HECHT M., PETERSEN M., STRELITZ R., MALTRUD M., AHRENS J., HLAWITSCHKA M., HAMANN B.: Visualization and analysis of eddies in a global ocean simulation. *Computer Graphics Forum 30*, 3 (2011), 991–1000. 4

[WZW*20] WOLLIGANDT S., ZIMMERMANN J., WILDE T., MOTEJAT M., THEISEL H.: Lagrangian q-criterion and transport of salt and temperature. IEEE Scientific Visualization Contest 2020. 2

[XLWD19] XIE C., LI M., WANG H., DONG J.: A survey on visual analysis of ocean data. *Visual Informatics 3*, 3 (2019), 113–128. 2

[ZBH*18] ZANNA L., BRANKART J., HUBER M., LEROUX S., PENDUFF T., WILLIAMS P.: Uncertainty and scale interactions in ocean ensembles: From seasonal forecasts to multi-decadal climate predictions. *Quarterly Journal of the Royal Meteorological Society 145* (10 2018). 2